Research Square

Preprints are preliminary reports that have not undergone peer review.
They should not be considered conclusive, used to inform clinical practice,
or referenced by the media as validated information.

Disturbance storm time index coupling with solar wind/IMF parameters

Geletaw Behailu Belayneh

geletawbphys@gmail.com

Research Article

Keywords: Dst index, Solar wind, XWT, WTC, Interplanetary magnetic field (IMF), time shifted cross correlation

Posted Date: November 4th, 2026

DOI: https://doi.org/10.21203/rs.3.rs-10047860/v1

License: This work is licensed under a Creative Commons Attribution 4.0 International License.
Read Full License

Additional Declarations: No competing interests reported.

Disturbance storm time index coupling with solar wind/IMF parameters

Geletaw Behailu Belayneh[1,2*]

[1*]Department of Physics, Bahir Dar University, Bahir Dar, Ethiopia.
[2]Washera Geospace and Radar Science Laboratory, BDU, Ethiopia.

Corresponding author(s). E-mail(s): geletawbphys@gmail.com;

Abstract

Understanding the complex coupling between the interplanetary magnetic field (IMF), solar wind dynamics and geomagnetic activity remains a cornerstone of space weather research. While the broader relationships are well-acknowledged, quantifying the precise, time-dependent impacts of specific heliospheric drivers on the Disturbance Storm Time ($\boldsymbol{Dst}$) index requires deeper investigation. This study systematically analyzes the interactions between the $\boldsymbol{Dst}$ index and a comprehensive suite of solar wind and IMF parameters-including velocity ($\boldsymbol{v_{sw}}$), density ($\boldsymbol{n_{sw}}$), dynamic pressure ($\boldsymbol{P_{sw}}$), convective electric field ($\boldsymbol{E_{sw}}$) and magnetic field components ($\boldsymbol{B_x}$, $\boldsymbol{B_y}$, $\boldsymbol{B_z}$, $\boldsymbol{B_{total}}$), alongside the $\boldsymbol{ap}$ and $\boldsymbol{AE}$ indices-using high-resolution data from 2010 to 2018. Employing a robust framework of Time-Shifted Cross-Correlation (TSCC), Cross Wavelet Transform (XWT) and Wavelet Transform Coherence (WTC), we map both the transient lags and localized periodicities of these interactions. TSCC analysis reveals a distinct zero-day lag response, characterized by strong negative correlations for $\boldsymbol{v_{sw}}$, $\boldsymbol{ap}$, $\boldsymbol{AE}$, $\boldsymbol{E_{sw}}$, $\boldsymbol{B_{total}}$ and $\boldsymbol{P_{sw}}$ against the $\boldsymbol{Dst}$ index, contrasted by positive correlations with $\boldsymbol{B_z}$, $\boldsymbol{n_{sw}}$ and the $\boldsymbol{v_{sw}B_z}$ coupling term. Furthermore, XWT and WTC analyses identify high common-power regions and phase-locked coherence dominated by a $\sim$28-day solar rotation periodicity across the driving parameters. These findings refine our understanding of solar-terrestrial energy transfer mechanisms and offer critical constraints for empirical geomagnetic storm forecasting models.

Keywords: Dst index, Solar wind, $\boldsymbol{XWT}$, $\boldsymbol{WTC}$, Interplanetary magnetic field ($\boldsymbol{IMF}$), time shifted cross correlation

1 Introduction

The magnetosphere is a very complex dynamical system for which it is very difficult to use first principles to derive an analytically set of equations that govern the evolution of this system. The magnetosphere can be considered as a complex input-output system [1]. To understand this complex systems, there are different approaches exist. It is possible to study each process involved in the dynamics of the whole system individually and then to conjugate these into a global model of the system. The other approach is to use the observations to study generic properties of the whole dynamical system and to derive a model of the system directly from these observations [2]. The Disturbance storm time (Dst) index is a measure used in space weather to quantify the intensity of magnetic storms caused by interactions between the solar wind and Earth's magnetic field [3]. It is derived from measurements of the horizontal component of Earth's magnetic field at several observatories located around the globe. These observatories record changes in the magnetic field caused by the solar wind's impact. The data from multiple observatories are combined to calculate the Dst index, which represents the deviation of the horizontal magnetic field from its expected quiet-time level. The magnitude of the Dst index reflects the severity of the storm, with more negative values indicating stronger disturbances. Scientists and space weather forecasters use the Dst index to monitor and predict the impact of geomagnetic storms on technological systems, such as power grids, satellites, and communication networks [3–5]. It helps assess the potential for disruptions and allows for mitigation measures to be taken when necessary. In this second approach, parameters of the solar wind and IMF parameters are considered as inputs to the magnetosphere and Dst index (other geomagnetic indices) are considered as outputs. This approach is exploited in the present work, with the aim of identifying the driving parameters or inputs by considering Dst index as an output in the system using statistical techniques.

The relationship between the Dst index and solar wind parameters has been extensively studied [6–10]. Siscoe et al. [6] discussed the relationship between solar wind parameters and the Dst index. They highlight the impact of southward IMF Bz on geomagnetic storms and the resulting negative excursions in the Dst index. They also emphasize the role of high solar wind speed and high-density conditions in enhancing the strength of geomagnetic disturbances. Lyon et al. [7] investigated the statistical connection between solar wind parameters and the Dst index during the declining phase of solar cycle 23. The researcher find that the Dst index is primarily driven by southward IMF Bz and solar wind dynamic pressure. The researcher also note the importance of the solar wind speed in determining the duration of geomagnetic storms. Tsurutani et al.[9] explored the relationship between solar wind parameters and intense geomagnetic storms. They identify the presence of long-duration southward IMF Bz events combined with high solar wind speed as a key driver of HILDCAA (high-intensity long-duration continuous AE activity) events, which often correspond to significant negative excursions in the Dst index. Numerous studies of correlation analysis between the solar wind parameters and Dst index show the product of the solar wind velocity and the southern component of the magnetic field gives highest value [2, 3]. Troshichev et al.[10] analyzed the correlation between the

Dst index and solar wind parameters using a large dataset. They find that the *Dst* index is strongly correlated with southward IMF Bz, solar wind speed, and dynamic pressure. They also identify a threshold value of solar wind speed above which the *Dst* index exhibits a more significant response to changes in IMF Bz. These studies, among many others, provide empirical evidence supporting the relationship between the *Dst* index and solar wind parameters. They highlight the importance of southward IMF Bz, solar wind speed, solar wind density, and dynamic pressure in influencing the intensity of geomagnetic storms and the resulting variations in the *Dst* index.

Wavelet analysis has been used to uncover the temporal variations of the solar wind/IMF and geomagnetic indices by different researchers [11–20]. Huang et al. [11] used wavelet analysis to investigate the periodicities in solar wind parameters. They identified significant periodicities ranging from a few minutes to several hours, corresponding to different physical processes and solar wind structures. Podladchikova et al.[17] applied the wavelet transform to study the time-varying behavior of IMF parameters. They found intermittent and sporadic variations at different scales, highlighting the complex nature of IMF fluctuations. Richardson et al. [15] employed wavelet coherence analysis to examine the coupling between IMF components and solar wind speed. They identified coherent oscillations at various scales, indicating the presence of Alfv?nic and magnetosonic waves. Torrence et al.[12] introduced wavelet-based power spectral analysis and applied it to examine the periodicities in geomagnetic indices. They revealed the presence of various oscillations, including the diurnal, semi-diurnal, and longer-period fluctuations. Huang et al.[11] employed wavelet coherence analysis to study the relationship between solar wind speed and the AE index, which represents the global geomagnetic activity. They identified significant coherence at different scales, indicating the coupling between solar wind and geomagnetic disturbances. Liu et al.[14] investigated the relationship between solar wind parameters and the Dst index using wavelet coherence analysis. They identified significant coherence at different timescales, indicating the influence of solar wind on geomagnetic disturbances. Gopinath et al.[16] utilized wavelet analysis to explore the multifractal properties of geomagnetic indices. They found evidence of multifractality, indicating the presence of complex and self-similar structures in the geomagnetic time series. These studies demonstrate the usefulness of wavelet analysis in uncovering temporal variations, identifying periodicities, and exploring the relationships between solar wind/IMF parameters, and geomagnetic indices. The technique allows for a detailed examination of the time-frequency characteristics, providing insights into the dynamic processes.

In this paper, we investigated the coupling of *Dst* index with solar wind/IMF parameters using three mathematical tools, which are time shifted cross correlation, cross wavelet transform and wavelet transform coherence. Wavelet coherence analysis allows for the examination of the coherence and phase relationships between different geomagnetic indices (such as *Dst* index) and solar wind/IMF parameters. This helps in understanding the coupling and interactions between different components of the Earth's magnetosphere-ionosphere system.

2 Data and Methodology

2.1 Data Sources

A number of Dst index predictive models were constructed using varying statistical methods of both linear and nonlinear processes by considering different solar wind and IMF parameters as input [21–25]. In most cases, the Dst index was used as the target variable to be predicted, while a number of solar wind and IMF parameters were employed as independent variables (these are Bx, By, and Bz components of the IMF and B_{total} in (nT), solar wind proton density in $N.cm^{-3}$, solar wind plasma speed in $km.s^{-1}$, and plasma flow pressure in (nPa), electric field (mV/m), and geomagnetic indices such as Geomagnetic Auroral Electrojet (AE) index or $AE\,(nT)$, and geomagnetic Ap index or $ap\,(nT)$). Thus, we used solar wind and IMF parameters and geomagnetic indices data to implement the time shifted cross correlation, cross wavelet transform and wavelet transform coherence analysis. A total of $N = 3285$ daily averages of solar wind, IMF and geomagnetic indices data were obtained from January 1, 2010 to December 31, 2018. All data was obtained from the GSFC (Goddard Space Flight Center)/SPDF (Space Physics Data Facility) OMNIWeb interface (http://omniweb.gsfc.nasa.gov/). This study has been performed by using ACE spacecraft measurements. ACE orbit at the L1 libration point, which is a point of the Earth-Sun gravitational equilibrium about 1.5 $million\ km$ from the Earth and 148.5 $million\ km$ from the Sun with a semi-major axis of approximately $200,000\,km$.

2.2 Methodology

This work is based on the time shifted cross correlation, the cross-wavelet transform (XWT) and wavelet transform coherence (WTC) analysis applied between the Dst index and solar wind/IMF parameters. Thus it is important to describe a simple introduction of these mathematical tools.

2.2.1 Time Shifted Cross Correlation ($TSCC$)

The common method to study causal relationship between two time series is to use a time - shifted cross correlation analysis, which is defined as

$$r(\tau, t) = \frac{X(t)Y(t+\tau) - \langle X\rangle\langle Y\rangle}{\sqrt{\langle X^2\rangle - \langle X\rangle^2}\sqrt{\langle Y^2\rangle - \langle Y\rangle^2}}, \tag{1}$$

where r is the correlation coefficient, $\langle \dots \rangle$ is an ensemble average obtained by drawing samples at a set of measurement times, $\{t_0, t_1, \dots, t_n\}$. The causal dependency of the two parameters can be identified from the time-shift of the peaks of cross-correlation indicating a response time. The correlation coefficient defined how well correlated the two series are varying from -1 to 1. When $r < 0$ it means that the correlation is negative, with -1 being the maximum negative correlation value which is perfect negative correlation. When $r > 0$, we have the positive correlation with 1 being the perfect positive correlation. When $r = 0$, it means that there is no correlation between the two series. The time shifted cross correlation is calculated by the displacement

of one series relative to the other by units of time (τ) which provides the lag of the correlation [26].

2.2.2 Wavelet Transform (WT)

The wavelet transform is an efficient method to evaluate non-stationary signals and the progression of each frequency over time [12]. The wavelet functions are generated by expression $\psi(t)$ over a given time (t) and the mother wavelet is given by $\psi_{a,b}(t) = \frac{1}{\sqrt{a}}\psi(\frac{t-b}{a})$, where a represents the scale associated with expression and contraction from the wavelet and b is the time localization. The Morlet wavelet is given by $\psi(t) = e^{i\xi_o t}e^{-t^2/2}$, where ξ_o is a dimensionless frequency. The wavelet transform applied on $f(t)$ time series is defined as

$$WT(a,b) = \int f(t)W^*_{(a,b)}(t)\,dt, \tag{2}$$

where $f(t)$ is a time series, $\psi_{a,b}(t)$ is the wavelet function and $\psi^*_{a,b}(t)$ represents the complex conjugate o the wavelet function. These wavelet transforms have been expanded to a bivariate wavelet analysis; cross wavelet (XWT) and wavelet coherence (WTC) that investigate the time frequency domain correlation between two signals for determining the phase angle between the time series.

2.2.3 Cross Wavelet Transform (XWT)

We used the cross wavelet transform to obtain the common periods between time series and also to study the temporal variability of the main period found [27]. The XWT is given by Grinsted et al. [13]

$$W^{YX}(a,b) = W^Y(a,b)W^X(a,b)^*, \tag{3}$$

where $W^{YX}(a,b)$ is the cross wavelet power spectrum, W^Y and W^X represent the wavelet transform coefficients applied on the time series $Y(t)$ and $X(t)$ respectively and $(*)$ represent the complex conjugate of the transform. Furthermore, a and b are the scaling and time translation parameters, respectively. We also used the global wavelet spectrum (GWS) that is used to identify the most energetic periods present on the cross wavelet analysis. The GWS is given by

$$GWS = \int |WT(a,b)|^2\,db \tag{4}$$

2.2.4 Wavelet Transform Coherence (WTC)

The wavelet transform coherence (WTC) is a sufficient tool for identifying the localized and quasi periodic variation. The WTC spectrum is used to determine how coherent the cross wavelet transform is in time-frequency space with more effectiveness at identifying time frequency correlation even areas where both time series have low power

compared to XWT. The cross wavelet coherence spectrum was defined by Grinsted et al. [13] as follows

$$R^2(a,b) = \frac{(S[a^{-1}W^{XY}(a,b)])^2}{S[a^{-1}W^{X}(a,b)]S[^{-1}W^{Y}(a,b)]}, \tag{5}$$

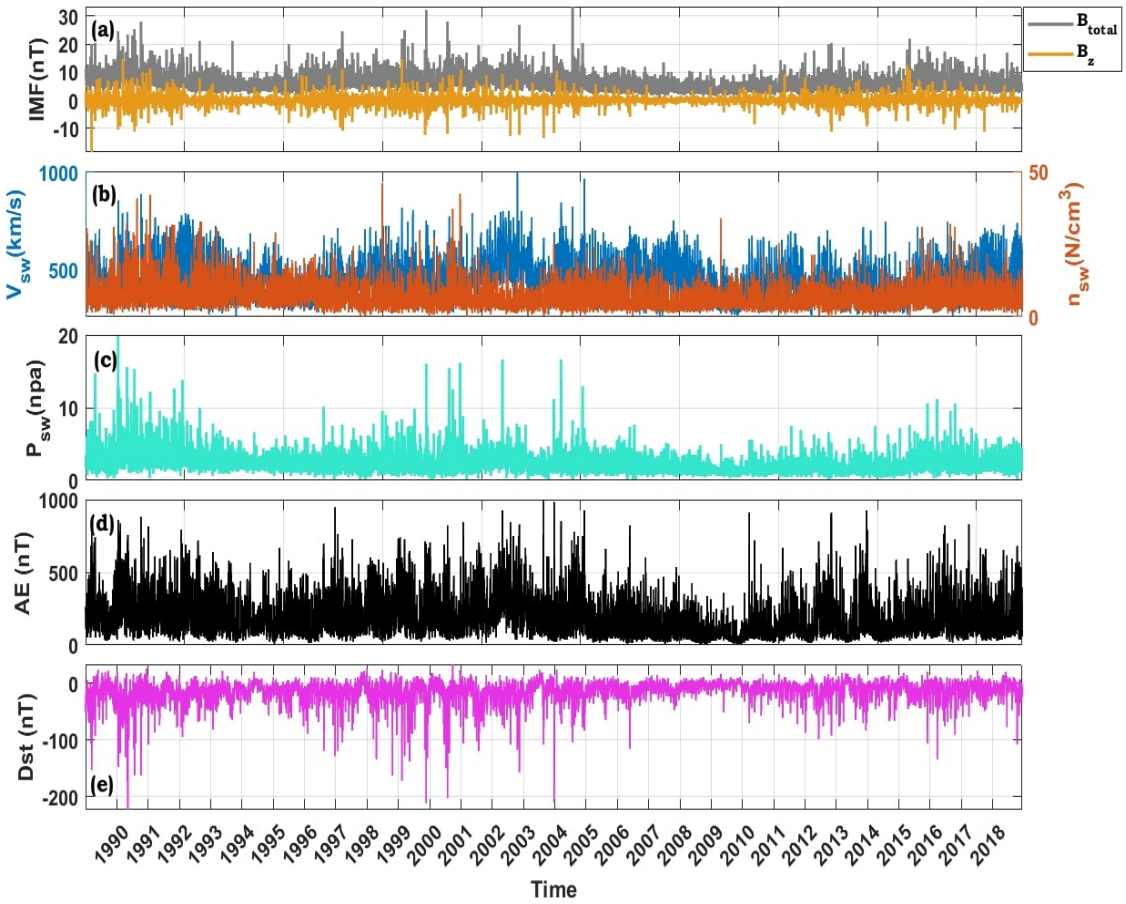
where S is the smoothing operator in this case and it is given by $S(W) = S_{scale}(S_{time}(W^{XY}(a,b)))$, where S_{scale} and S_{time} denote smooth along the wavelet scale axis and smoothing in time, respectively [12, 13, 17]. Since this is identical to that of the conventional correlation coefficient, the wavelet coherence can be treated as a correlation coefficient localized in the time frequency space. The WTC value around 1 indicate a higher degree of resemblance across time series, while coherence value near 0 indicate no correlation.

We have applied the above mathematical tools for the solar wind and IMF parameters (solar wind dynamic pressure (p_{sw}), solar wind density (n_{sw}), electric field (E_{sw}) IMF B_{total}, IMF B_x, B_y, B_z components, AE and ap) to understand dependency on variations of Dst index. These observations can help us to understand relationship between the solar wind/IMF variables into ring current or Dst index. In order to analyze the time series data of Dst index and solar wind/IMF parameters, the time resolution of these data systems must be the same. In this work, we investigated quantitative relationship between Dst index and solar wind/IMF parameters.

3 Results and Discussions

3.1 Observations

Figure 1 shows the temporal variations of solar wind and IMF parameters, and also geomagnetic indices during the period from 01 January 2010 - 31 December 2018. Panel (a) shows the variations of total IMF values (gray) and IMF B_z component (orange). B_{total} value of the interplanetary magnetic field indicates the total strength of the interplanetary magnetic field and its value varied from 0 to $30\,nT$, whereas B_z component varied from $-20\,nT$ to $20\,nT$. Panel (b) illustrates the variation of solar wind velocity and solar wind density. The maximum solar wind velocity has been observed about $\sim$ $1003\,km/s$ whereas the maximum solar wind density is about $\sim$ $45.9\,N/cm^3$. Panel (c) demonstrates the variation of flow pressure and its maximum value is about $\sim$ $19.9\,nPa$. In a similar way, panel (d) demonstrates the temporal variations of AE index with the maximum value becomes $993nT$. Figure 1 last panel (e) shows the temporal variations of the Dst-index. This panel shows that the Dst index is highly variable in time and its minimum value reaches to $-223\,nT$ during the strong geomagnetic storm time. Moreover, Figure 1 illustrates that the strength of variations in solar wind/IMF parameters as well as magnetic index (AE index) corresponds with the variations in Dst index.



1

Fig. 1 Observation of solar wind, IMF parameters and geomagnetic indices in the period from 01 January 2010 - 31 December 2018. (a) IMF B_{total} (gray) and B_z component (orange), (b) Solar wind velocity, v_{sw} (Blue) and density, n_{sw} (red), (c) Flow pressure, P_{sw} (white-green), (d) AE index (black), (e) Dst index (magenta).

3.2 Cross Correlation

Figure 2 shows the scatter plot to check the cross correlation of solar wind and IMF parameters, including some geomagnetic indices with that of Dst index. In each panel the linear fitting function as well as the cross correlation coefficients are presented. The least cross correlation coefficient were observed in the IMF components Bx and By with values of 0.011 and 0.014, respectively. Thus, the coupling function between solar wind and Dst is insignificantly dependent on Bx and By of IMF. The maximum correlation coefficients were recorded between Dst index and ap and AE indices with values of 0.754 and 0.707, respectively. The IMF Bz, solar wind density, and BV (the product of solar wind speed and Bz south component) are positively correlates with Dst index. The rest of the solar wind/IMF parameters and also geomagnetic indices negatively correlates with Dst index. The cross correlation does not provide any way

to clearly distinguish between two variables that are passively correlate because of a common driver rather than causally related. Dst index is an hourly index that gives a measure of the strength of the symmetric ring current that, in turn, provides a measure of the dynamics of geomagnetic storm. Studies have shown that the electric field, BV (v_{sw} $\times$ southward IMF Bz) has a strong effect on the ring current dynamics [28–30].

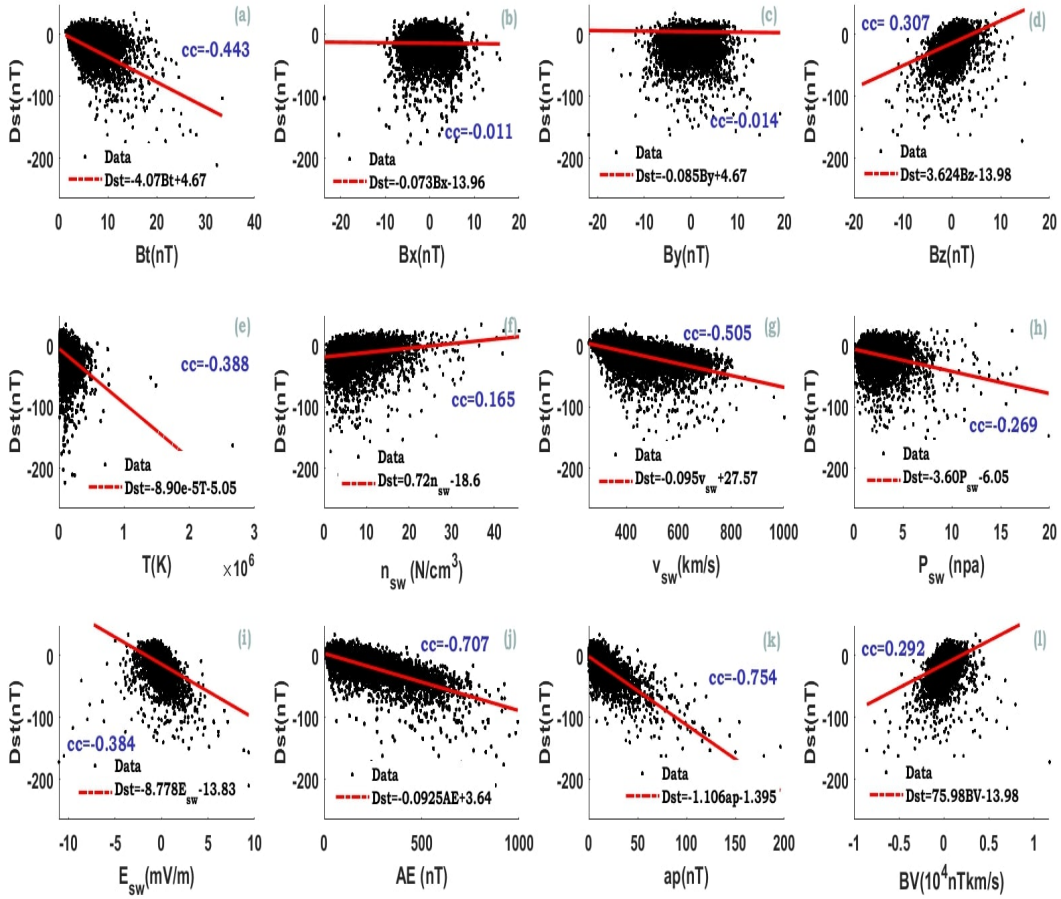


Fig. 2 Scatter plot for cross correlation anlysis i.e. panels (a) Dst vs B_{total}, (b) Dst vs B_x, (c) Dst vs B_y, (d) Dst vs B_z, (e) Dst vs T, (f) Dst vs n_{sw}, (g) Dst vs v_{sw}, (h) Dst vs P_{sw}, (i) Dst vs E_{sw}, (j) Dst vs AE, (k) Dst vs ap, (l) Dst vs BV in the period from 01 January 2010 - 31 December 2018. cc indicates the correlation coefficient value.

Figure 3 shows the time-shifted cross-correlation functions of solar wind and IMF paremeters and also geomagnetic indices with that of Dst index. The result illustrates that the cross-correlation coefficients as a function of lag time depends on the types of driving parameters. It shows that Dst index is positively correlated with BV, Bz and solar wind density (n_{sw}) and anticorrelated (negative correlated) with AE index, ap index, solar wind velocity (v_{sw}), B_{total} as well as with solar wind pressure. As shown in Figure 3 the cross-correlation coefficients peak value corresponds to spacific lag time, which is almost similar for postively correlated driving parametere, at about zero lag time. For parameters which are negatively correlated the peak correlation cofficient correponds to 1 day for B_{total} and P_{sw} and at about zero lag time for the rest of the parameters. Previous papers discussed the physical relation between AE index and the Dst index and also other solar wind parameters [31–33]. The time-shifted cross correlation coefficient values observed for IMF B_x, B_y, and electric field are too weak and so the relation of those parameters with Dst index become insignificant. In these parameters the correlation coefficients are nearly zero and hence no correlational relation observed for these parameters with geomagnetic index (Dst). In a similar way, Zhu et al.[1] confirmed that there is poor correlation between solar wind electric field and ring current. As shown in Figure 3 the variation of correlation coefficient in lag time depends on the kind of driving parameters. So, it shows the rank of driving parameters with respect to time-shifted cross correlation coefficient values. Thus, AE index and ap index play the dominant role in the variations of Dst index. The reason might be related with being they are also the geomagnetic indices as Dst index. B_z and BV parameters are positively correlated with Dst index and the correlation relation declines as the lag time increases. B_t and P_{sw} show peak correlation coefficient with one day lag time. They are found to be negatively correlated with Dst index. Whereas, BV and Bz are in second place for their role in the Dst index variations.

This cross-corelation result is consistent with the previous results of Burton et al. [21], Zhu et al. [1] and Boaghe et al. [32] although we have used different data sets. Although the correlation coefficients are weak, the correlation coefficient values of AE, v_{sw}, n_{sw}, ap and BV are highly significant (significance level: $P < 10^{-2}$) due to the large number of data points. Since cross-correlation studies only detect linear relationships, so if the feedback involves nonlinear processes then their usefulness may be seriously limited. Wavelet analysis provides a comprehensive understanding of the temporal and spectral characteristics of solar wind, IMF parameters, and geomagnetic indices and nonlinear relationships in dynamical system. It helps in studying the dynamics of the Sun-Earth system, investigating the impact of solar disturbances on the Earth's magnetosphere, and improving space weather forecasting. Wavelet analysis aids in identifying and characterizing different physical processes, such as magnetospheric responses to solar wind variations. It is a valuable tool for studying the time-frequency properties, periodicities, coupling, and correlations within the solar wind-IMF-geomagnetic system. It enhances our understanding of space weather dynamics and helps in developing strategies for space weather monitoring, prediction, and mitigation. Thus, in this study we used cross wavelet transform and wavelet transform coherence to understand the coupling between the Dst index and solar wind parameters and the results are discussed in the next subsection.

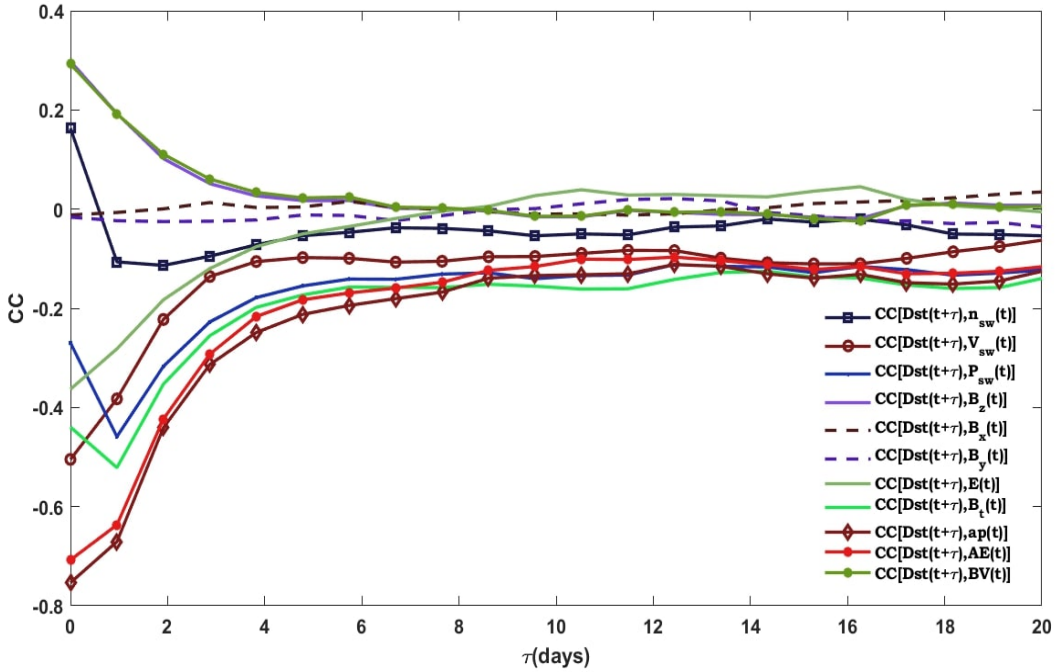


Fig. 3 Time-shifted cross-correlation coefficients of solar wind and IMF parameters with Dst index ($Corr[v_{sw}(t), Dst(t+\tau)]$, $Corr[n_{sw}(t), Dst(t+\tau)]$, $Corr[p_{sw}(t), Dst(t+\tau)]$, $Corr[B_z(t), Dst(t+\tau)]$, $Corr[B_x(t), Dst(t+\tau)]$, $Corr[B_y(t), Dst(t+\tau)]$, $Corr[E_{sw}(t), Dst(t+\tau)]$, $Corr[ap(t), Dst(t+\tau)]$, $Corr[AE(t), Dst(t+\tau)]$ and $Corr[BV(t), Dst(t+\tau)]$) during the period from 01 January 2010 - 31 December 2018.

3.3 Cross wavelet Transform (XWT)

The XWT is very useful technique to examine synchronization and phase asynchronous between two time series in time frequency space. Figure 4 show the XWT between the IMF parameters and Dst index which means panel (a) XWT between Dst and Bx, panel (b) XWT between Dst and By, panel (c) XWT between Dst and Bz, and panel (d) XWT between Dst and Bt (total IMF). As mentioned earlier, the XWT is calculated from the two time series wavelet transform, so it identifies regions of high common power between two physically related time series data. The cross-wavelet power spectra between Dst and Bx, show significant common power in the multiple bands, mostly at 28 days in the year 2010, 2011, 2013, and from 2015 - 2017 remaining at about 512 days in the regions from 2013 - 2016. Similarly, the cross-wavelet power spectra between Dst and By, also show significant common power in the multiple bands, mostly at 28 days in the year 2010, 2011, 2013, and from 2015 - 2017 remaining at about 512 days in the regions from 2012 - 2016. Whereas the cross-wavelet power spectra between Dst and Bz show significant common power in the multiple bands like 28 days in 2012, 2015, 56 days in 2012, 128 days from 2012 - 2013, 156 days in 2011, about 350 days from 2013 - 2015 and 512 days from 2012 - 2015. The cross-wavelet power spectra between Dst and Bt show significant common power

in the multiple bands like 28 days in 2013, 2016, 128 days from 2012 - 2013, about 350 days from 2013 - 2015 and 512 days from 2012 - 2015. Similar patterns were also observed for XWT of Dst with Bx and By. Also, the thick black lines clearly indicate the 5% significance level, and it is worth mentioning that the area of a time-frequency plot is a reliable measure of causality when the significance level is less than or equal to 5%.

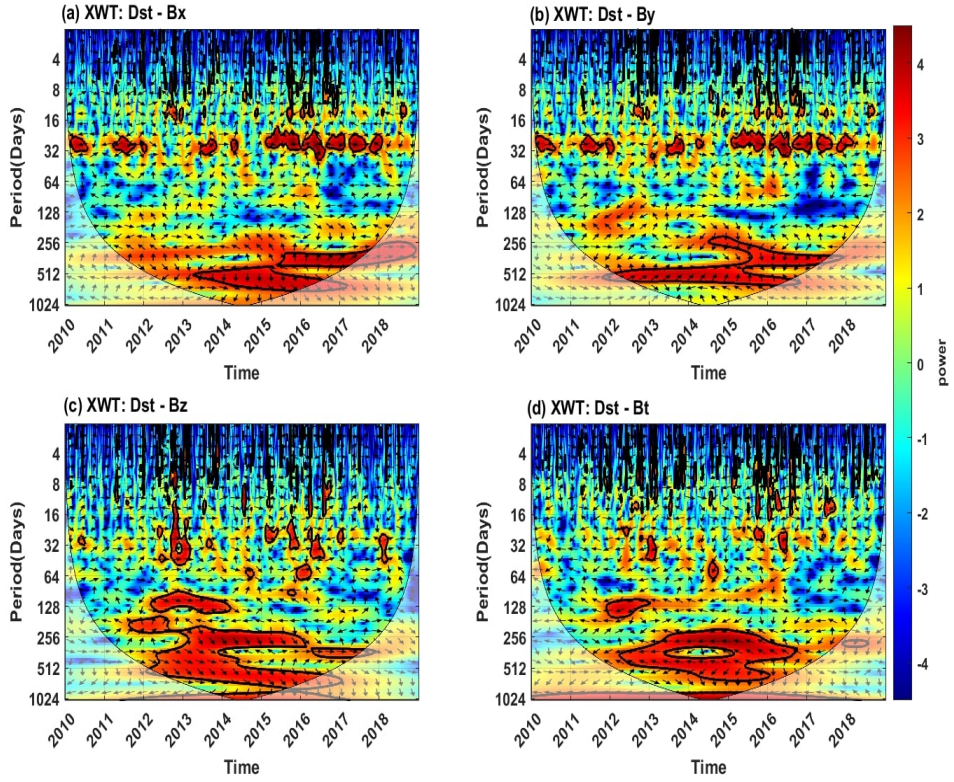


Fig. 4 The XWT of the Dst index and IMF parameters which means (a) XWT between Dst and Bx, (b) XWT between Dst and By, (c) XWT between Dst and Bz, and (d) XWT between Dst and Bt (total IMF) during the period from 01 January 2010 - 31 December 2018.

Figure 5 show the XWT between the solar wind parameters and Dst index which means panel (a) XWT between Dst and n_{sw}, panel (b) XWT between Dst and v_{sw}, panel (c) XWT between Dst and P_{sw}, and panel (d) XWT between Dst and E_{sw}. As Figure 5 (a) shown the cross-wavelet power spectra between Dst and n_{sw}, also show significant common power in the multiple bands, mostly at 14 days in the year 2016, 2017, 28 days in 2011, and from 2015 - 2017, 56 days in 2012, about 350 from 2012 - 2016 and the remaining at about 512 days in the regions from 2012 - 2016. Whereas the cross wavelet power spectrum between Dst and v_{sw} shows that there are significant common power in the multiple bands which means 14 days in 2012, 2015, 2017, 28 days in 2010, and from 2015 - 2017, 136 days in 2012, about 350 days from 2011 - 2015 and 512 days from 2012 - 2015. In a similar manner the cross wavelet power spectrum between Dst and P_{sw} gives multiple bands which are 14 days in 2015, 28 days in 2015 and 2016, 56 days in 2016, 128 days in 2012, about 350 days from 2012 - 2017 and about 512 days from 2012 - 2015. Similarly, the cross wavelet power spectrum between Dst and E_{sw} gives multiple bands which are 28 days in 2011, 2012, and from 2015 - 2018, 128 days from 2012 - 2014, 156 days from 2012 - 2016, about 350 days from 2012 - 2017 and about 512 days from 2012 - 2016.
Wavelet-based cross-correlation technique enables the investigation of the time-delayed relationships and lag times between solar wind variations, IMF fluctuations, and subsequent geomagnetic responses. This aids in studying the propagation and transmission of solar wind disturbances towards the Earth. The wavelet analysis provides a powerful tool for exploring the temporal and spectral characteristics, periodicities, transient events, and correlations within the solar wind-IMF-geomagnetic system. It enhances our understanding of the underlying physical processes and interactions, contributing to space weather research and forecasting efforts.
Table 1 summarizes the XWT periodicity for Dst index and solar wind parameters (n_{sw}, v_{sw}, P_{sw}, E_{sw}) and interplanetary magnetic field parameters (B_x, B_y, B_z and B_t) and also geomagnetic indices (ap, AE) over the period from 2010 - 2018. The time span of each periodicity is also tabulated. This study identified significant coherence at different timescales, and indicating the existence of periodicities and correlations between solar wind variations and the Dst index.

3.4 Global wavelet spectrum (GWS)

Figure 6 show the peaks observed in the GWS which is the main periodicities associated with XWT of Dst and IMF parameters that is panel (a) Dst - Bx, panel (b) Dst - By, panel (c) Dst - Bz and panel (d) Dst - Bt. It is evident the abrupt changes in the Dst show significant periodicities in each IMF parameters. For XWT of Dst with B_x and B_y the peak period is 28 days. Moreover, for XWT of Dst with B_z and B_t there are multiple peaks in periodicity. (summarized in Table 2)
Figure 7 show the peaks observed in the GWS which is the main periodicities associated with XWT of Dst and solar wind parameters that is panel (a) Dst - n_{sw}, panel (b) Dst - v_{sw}, panel (c) Dst - P_{sw} and panel (d) Dst - E_{sw}. It is evident the abrupt changes in the Dst show significant periodicities in each solar wind parameters. For XWT of Dst with n_{sw}, E_{sw} and v_{sw} the peak period is about 28 days. Moreover, for

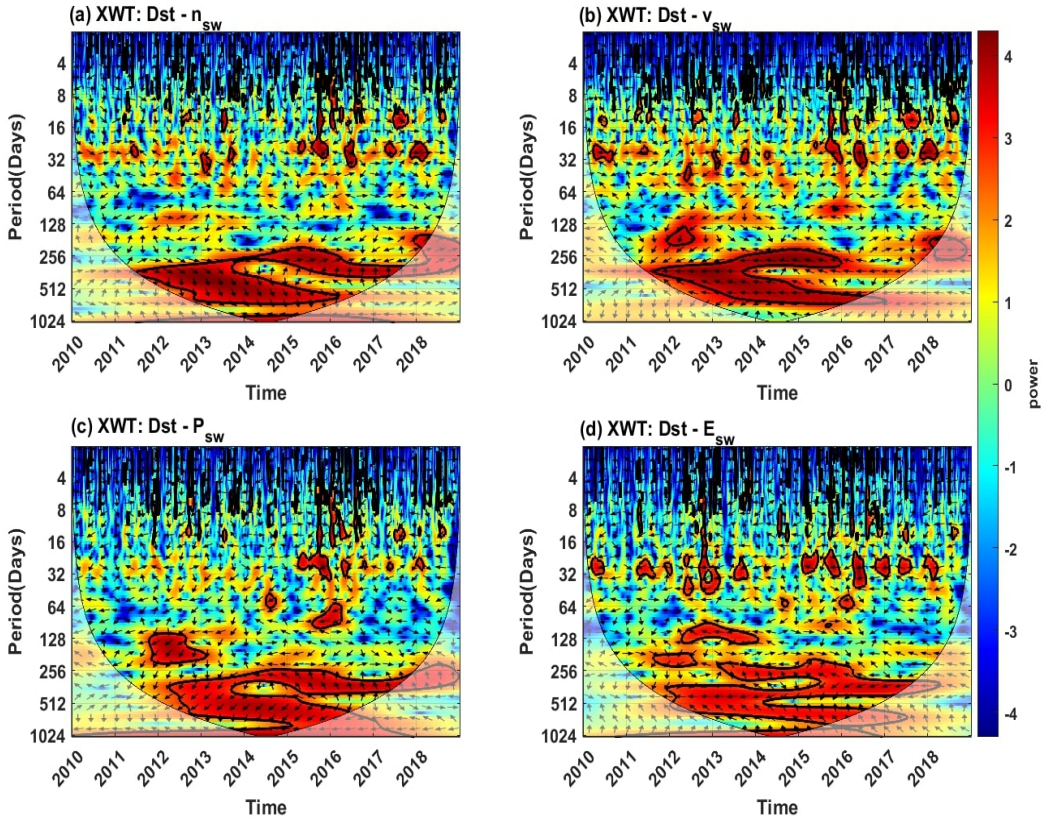


Fig. 5 The XWT of the Dst index and solar wind parameters which means (a) XWT between Dst and n_{sw}, (b) XWT between Dst and v_{sw}, (c) XWT between Dst and P_{sw}, and (d) XWT between Dst and E_{sw} during the period from 01 January 2010 - 31 December 2018.

XWT of Dst with P_{sw} there are multiple peaks as periodicity. (summarized in Table 3)

3.5 Wavelet Transform Coherence *WTC*

Figure 8 show results from WTC analysis, the coherency of XWT analysis was identified and the potential relationship between Dst and IMF parameters which means panel (a) WTC between Dst and Bx, panel (b) WTC between Dst and By, panel (c) WTC between Dst and Bz, and panel (d) WTC between Dst and Bt (total IMF) during the period from 01 January 2010 - 31 December 2018. It posses the in phase relationship with the interplanetary magnetic field components with Dst index. The potential relationship between Dst and IMF components varied with the intensity. WTC analysis of Dst index reveals distinct patterns of coherence and phase relationships across a spectrum of frequencies, underscoring dynamic coupling between solar wind conditions and geomagnetic responses. Wavelet coherence analysis is particularly

Table 1 XWT of significant periodicities for the Dst index and solar wind (including IMF) paarameters under study

Parameters	Periods (days)	Time span
Dst-Bx	28	2010-2018
	14	2012 and 2015 - 2016
	512	2013 - 2016
Dst-By	28	2010-2018
	14	2012 and 2016 - 2017
	250	2015 - 2018
	512	2012 - 2016
Dst-Bz	28	2012-2013 and 2015 - 2016
	128	2012 - 2014
	64	2015
	256	2012 - 2015
Dst-Bt	28	2012-2013 and 2015 - 2016
	128	2012 - 2013
	512	2012 - 2016
Dst-n_{sw}	28	2011-2018
	56	2013 - 2016
	512	2012 - 2017
Dst-v_{sw}	28	2011-2018
	64	2013
	256	2012 - 2013
	512	2012 - 2016
Dst-P_{sw}	28	2015-2017
	64	2014
	128	2012 - 2013 and 2015 - 2016
	256	2012 - 2013
	512	2013 - 2017
Dst-E_{sw}	28	2010-2018
	128	2012 - 2014
	256	2012 - 2017
	512	2012 - 2017
Dst-ap	28	2010-2018
	14	2016 - 2017
	128	2012 - 2013
	256	2014 - 2016
	512	2012 - 2015
Dst-AE	28	2010-2018
	64	2016
	128	2012 - 2014
	256	2012 - 2017
	512	2012 - 2017

useful for studying the coupling and correlations between solar wind, IMF parameters, and geomagnetic indices. It allows researchers to examine the strength and phase relationships between these variables at different scales. The identification of coherent oscillations through wavelet coherence analysis indicates the presence of physical connections and energy transfer between the solar wind, IMF, and geomagnetic indices (Dst).

Figure 9 show results from WTC analysis, the coherency of XWT analysis was identified and the potential relationship between Dst and solar wind parameters which

Table 2 Shows the peak periodicity from the GWS.

Parameters computed in GWS	Peak periodicity (days)
Dst - *Bx*	14, 28 and 256
Dst - *By*	14, and 28
Dst - *Bz*	6, 14, 28, 56, 126 and 256
Dst - *Bt*	6, 14, 28, 56, 126 and 256

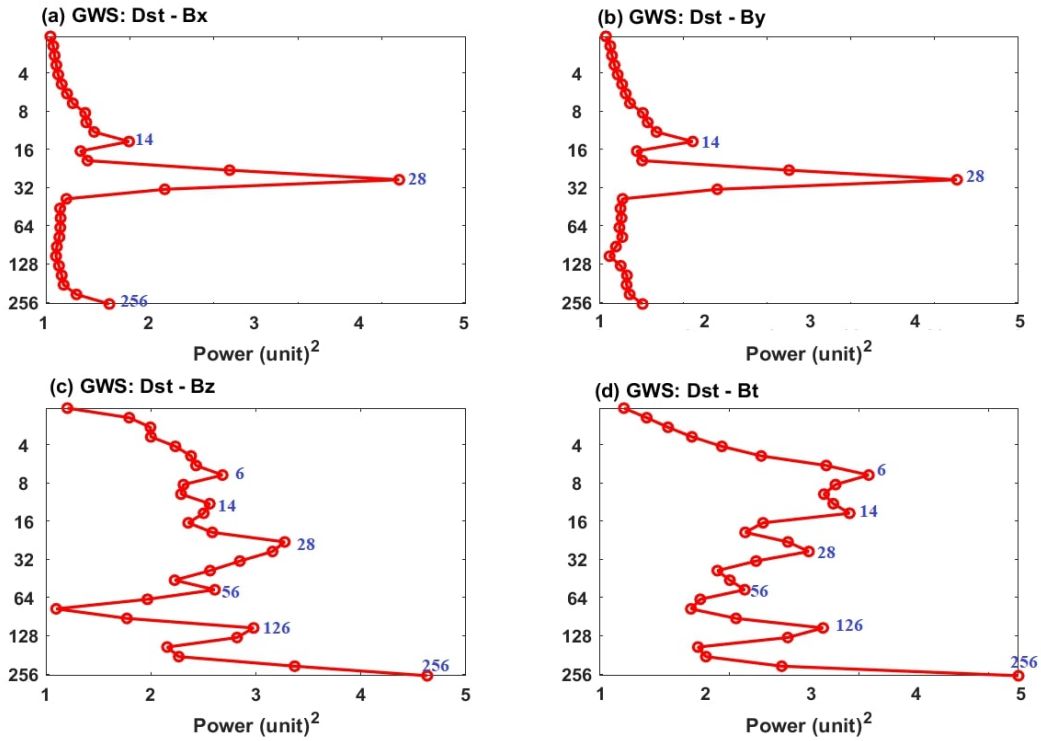


Fig. 6 The GWS of the *Dst* index and IMF parameters which means (a) GWS between *Dst* and *Bx*, (b) GWS between *Dst* and *By*, (c) GWS between *Dst* and *Bz*, and (d) GWS between *Dst* and *Bt* (total IMF) during the period from 01 January 2010 - 31 December 2018

means panel (a) WTC between Dst and n_{sw}, panel (b) WTC between Dst and v_{sw}, panel (c) WTC between Dst and P_{sw}, and panel (d) WTC between Dst and E_{sw} during the period from 01 January 2010 - 31 December 2018. It posses the in phase relationship with the solar wind parameters with Dst index. The potential relationship between Dst and solar wind parameters varied with the intensity. The study illustrates the application of wavelet analysis in studying the relationship between solar wind parameters and the Dst index. Wavelet coherence analysis has been particularly useful in identifying the strength and phase relationships between these variables at different scales, uncovering periodicities, and providing insights into the underlying physical processes driving geomagnetic storms.

Table 3 Shows the peak periodicity from the GWS.

Parameters computed in GWS	Peak periodicity (days)
Dst - n_{sw}	6, 14, 28 and 256
Dst - v_{sw}	14, 28 and 256
Dst - p_{sw}	6, 14, 28, 128 and 250
Dst - E_{sw}	14, 28, 54, 128 and 254

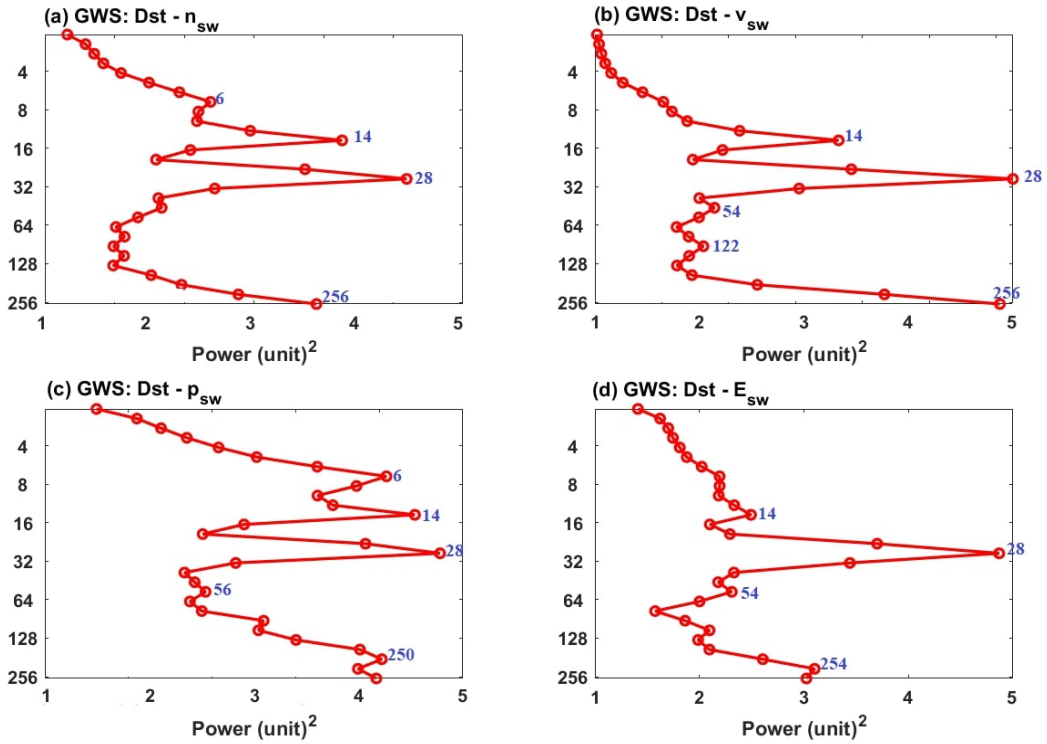


Fig. 7 The GWS of the Dst index and solar wind parameters which means (a) GWS between Dst and n_{sw}, (b) GWS between Dst and v_{sw}, (c) GWS between Dst and P_{sw}, and (d) GWS between Dst and E_{sw} during the period from 01 January 2010 - 31 December 2018.

The Dst index is influenced by various factors, primarily driven by the solar wind parameters. The IMF Bz, plays a crucial role in influencing the Dst index. When the IMF Bz is southward (negative), it has a stronger connection with Earth's magnetic field, allowing for more efficient energy transfer from the solar wind to the magnetosphere. This can lead to enhanced geomagnetic activity and more negative Dst values. Our results agree with this point that IMF Bz show positive correlation and the transfer entropy and also the mutual information show higher value next to the geomagnetic indices. Higher solar wind speeds generally increase the likelihood of geomagnetic storms. Faster solar wind can compress Earth's magnetosphere and generate stronger interactions with the magnetic field, resulting in more significant

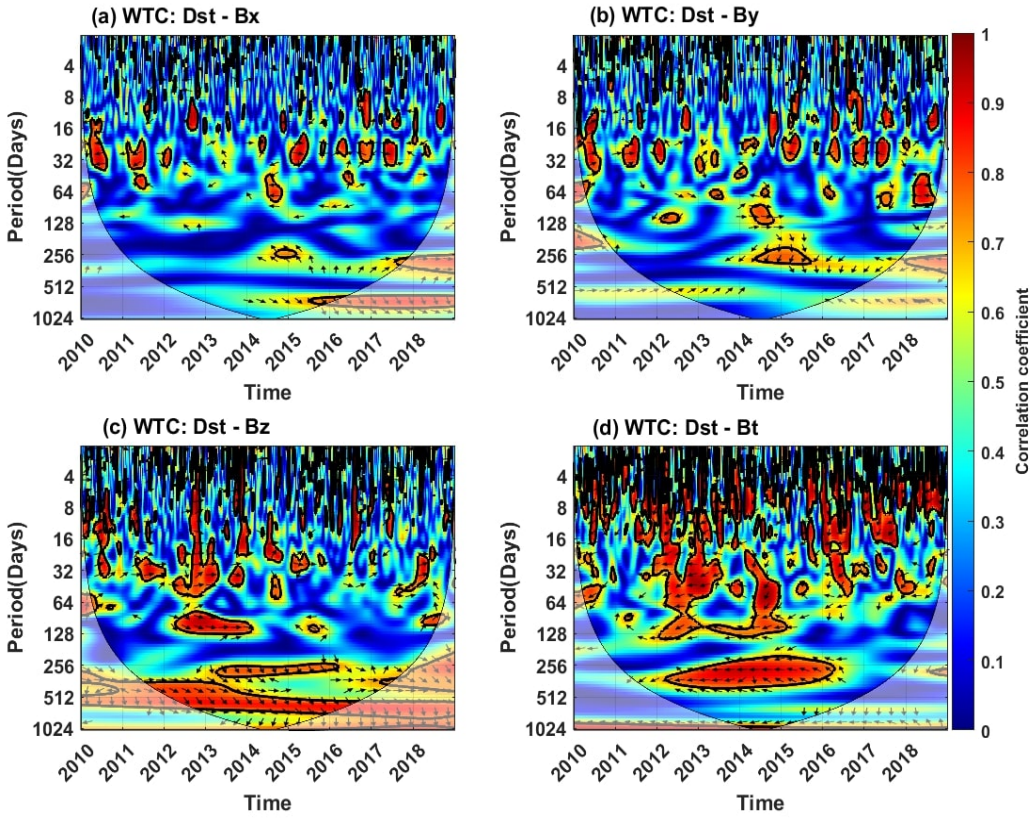


Fig. 8 The WTC of the Dst index and IMF parameters which means (a) WTC between Dst and Bx, (b) WTC between Dst and By, (c) WTC between Dst and Bz, and (d) WTC between Dst and Bt (total IMF) during the period from 01 January 2010 - 31 December 2018.

disturbances and negative Dst values. The density and pressure of the solar wind plasma can affect the intensity of geomagnetic storms. High - density and high - pressure conditions can enhance the coupling between the solar wind and Earth's magnetosphere, leading to more severe disturbances and lower Dst values. The sector structure of the IMF refers to the alternating regions of positive and negative magnetic polarity carried by the solar wind. Geomagnetic storms tend to be more intense and frequent when there are sustained periods of southward IMF Bz combined with a long duration of negative polarity. This configuration allows for prolonged and efficient energy transfer, resulting in more negative Dst values. It's important to note that the relationship between solar wind parameters and the Dst index is complex, and other factors, such as the arrival time of interplanetary shocks and the presence of magnetospheric substorms, can also influence geomagnetic activity. Space weather models combine these various factors to provide forecasts and estimates of the Dst index based on real-time solar wind measurements.

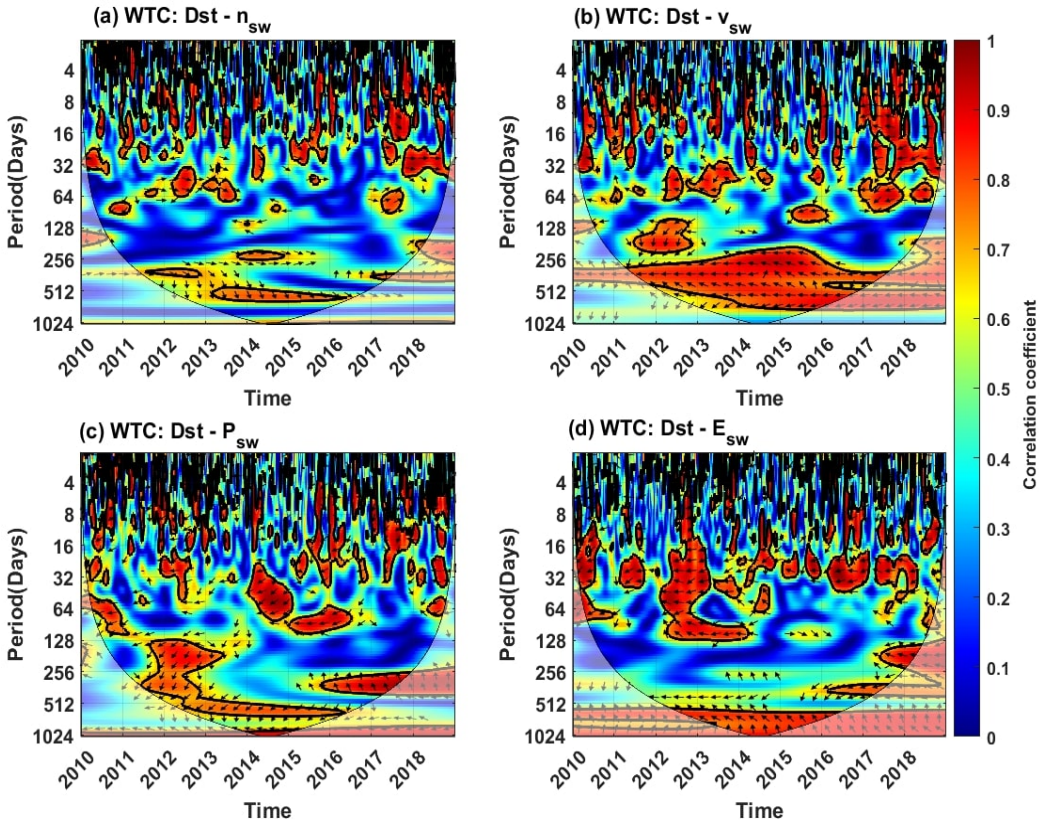


Fig. 9 The WTC of the Dst index and solar wind parameters which means (a) WTC between Dst and n_{sw}, (b) WTC between Dst and v_{sw}, (c) WTC between Dst and P_{sw}, and (d) WTC between Dst and E_{sw} during the period from 01 January 2010 - 31 December 2018.

Figure 10 shows the comparison of the XWT and WTC of the Dst index and geomagnetic indices which means panel (a) XWT between Dst and Ap, panel (b) XWT between Dst and AE, panel (c) WTC between Dst and Ap, and panel (d) WTC between Dst and AE during the period from 01 January 2010 - 31 December 2018. Figure 10 indicated that the WTC shows high cross wavelet coherence and in phase relationship for the computation between Dst and ap as well as Dst and AE geomagnetic indices. WTC is powerful statistical tool for analyzing two time series nonlinear behavior and determining significant coherence despite low common power. The WTC analysis can be used to determine the local correlation between two time series in time - frequency space. The thick back contours show the 95% confidence level in the wavelet power spectrum using Monte carlo simulations with a phase randomized surrogate series [13]. In order to separate locations with reliable and less accurate estimations, a cone of influence (COI) is inserted where edge effects might distort the picture. Arrow depict the relative phase relationship (in phase pointing right and anti phase pointing left.) From the analysis of WTC, the local correlation, time delay, and

phase structure between the two time series in time-frequency space can be explored. WTC finds locally phase-locked behavior, where XWT unveils high common power. XWT and WTC results point to the fact that these approaches provide an alternative way of assessing the coupling of Dst with solar wind and IMF parameters and also geomagnetic storm indicators and could be used as a sophisticated tool to forecast the emergence of these unique events by tracking short and long term variations in the solar wind parameters and relative deviations in Dst index.As can be seen in Figure 10 panels (c) and (d) there is high value of WTC or high percentage of correlations were observed for the ap and AE with Dst index pair at any geomagnetic conditions. The ring current index Dst is observed to have a greater influence on ap and AE during geomagnetic storm periods. It shows that strong coherence between AE/ap and the Dst index at several timescales.

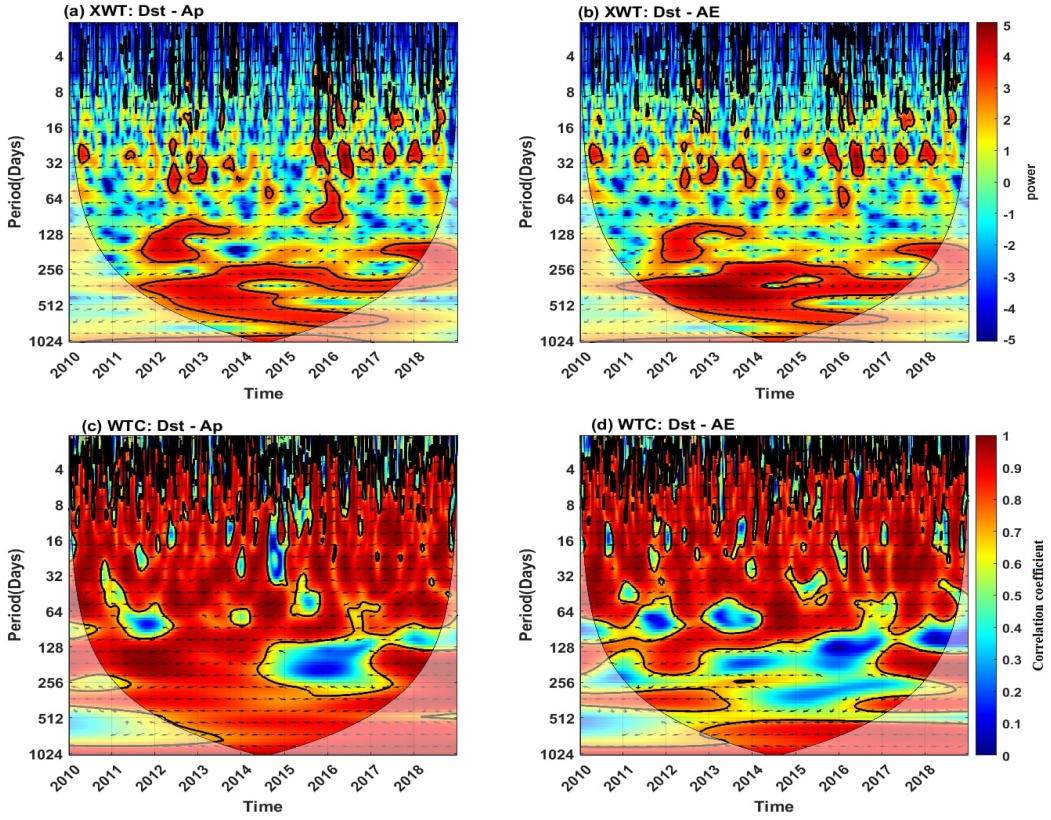


Fig. 10 Comparison of the XWT and WTC of the Dst index and geomagnetic indices which means (a) XWT between Dst and Ap, (b) XWT between Dst and AE, (c) WTC between Dst and Ap, and (d) WTC between Dst and AE during the period from 01 January 2010 - 31 December 2018.

4 Conclusion

In this work, we investigated the coupling of solar wind and IMF parameters with Dst index using three mathematical tool; time shifted cross correlation, cross wavelet transform and wavelet transform coherence. In order to understand the relationship between driving parameters and magnetosphere coupling response we have used 9 years data (from 01 January 2010 to 31 December 2018). We have applied the time shifted cross correlation, cross wavelet transform and wavelet transform coherence mathematical tools to identify the effect of driving parameters on Dst index. Time shifted cross correlation, cross wavelet transform and wavelet transform coherence analysis results are crucial to detect the driving parameters of ring current variation (Dst-index). The following points are our summarized results:

- From $TSCC$ analysis, the v_{sw}, ap, AE, E_{sw}, B_t and P_{sw} are negatively correlated, whereas B_z, n_{sw}, BV (solar wind speed times B_z) are positively correlated with Dst index with lag time of zero day.
- From XWT analysis, the high common power regions in wavelet spectrums with common periodicities of about 28 days were obtained for Dst and solar wind/IMF parameters during the period from 01 January 2010 to 31 December 2018. XWT revealed the key periodicities at almost all driving parameters of the Dst index which are the IMF and solar wind parameters. Thus, XWT analysis provides a comprehensive background for understanding the coupling between Dst and solar wind/IMF parameters.
- From WTC analysis, the coherency of XWT analysis was identified, and the potential relationship between Dst index and solar wind/IMF parameters and also geomagnetic indices(ap andAE) was uncovered. Coherence between solar wind/IMF components and the Dst index also exhibited significant variations at different frequencies, suggesting the involvement of distinct magnetospheric processes in storm generation. The results show that Dst index possesses in-phase relationship with all the above-mentioned parameters especially the WTC is strong between Dst index and ap and AE.

From the above results, we noticed that the correlation lag time as well as the strength of information transfer from solar wind/IMF parameters to Dst index depends on the types of driving parameters. Wavelet analysis has been employed to examine the temporal variations, periodicities, and correlations between solar wind parameters and the Dst index. The study's finding will demonstrate the suggested method are simple, effective and robust method for gaining deeper insight into the complex spatiotemporal characteristics of time series of Dst and solar wind parameters. The findings of information transfer from one parameter to another and the response lag time can provide insights into the physical relationships among parameters and solve constraints to models.

Data availability. Solar wind and IMF data were obtained from GSFC/SPDF OMNIWeb interface at http://omniweb.gsfc.nasa.gov, which are derived from ACE wind, Geotail and IMP-8 solar wind plasma and magnetic field observations. So the data is freely available in the above data archive.

Acknowledgements. The author thank all teams who are working on facilitating the data sources to be available for public user. He thank NASA/GSFC's Space Physics Data Facility's OMNIWeb (or CDAWeb) service and OMNI database. Solar wind and IMF data were obtained from GSFC/SPDF OMNIWeb interface at http://omniweb.gsfc.nasa.gov, which are derived from ACE wind, Geotail and IMP-8 solar wind plasma and magnetic field observations. He would like to acknowledge all sort of supports from Bahir Dar University.

Author contributions statement

G.B.: conceptualization, methodology, software, validation, formal analysis, investigation, resources data process, writing-original draft, writing-review and editing, visualization.

Funding

For this project no specific funding allocated.

Competing interests

The author declare no competing interests.

Additional information

Correspondence and requests for materials (codes) should be addressed to G.B. No ethical issues on this paper.

References

[1] Zhu, D., Billings, S., Balikhin, M., Wing, S., Alleyne, H.: Multi-input data derived dst model. Journal of Geophysical Research: Space Physics **112**(A6) (2007)

[2] Wei, H.-L., Billings, S.A., Balikhin, M.: Prediction of the dst index using multiresolution wavelet models. Journal of Geophysical Research: Space Physics **109**(A7) (2004)

[3] Gonzalez, W., Joselyn, J.-A., Kamide, Y., Kroehl, H.W., Rostoker, G., Tsurutani, B.T., Vasyliunas, V.: What is a geomagnetic storm? Journal of Geophysical Research: Space Physics **99**(A4), 5771–5792 (1994)

[4] Cowley, S.W.: The earth's magnetosphere: A brief beginner's guide. Eos, Transactions American Geophysical Union **76**(51), 525–529 (1995)

[5] Hajra, R., Echer, E., Tsurutani, B.T., Gonzalez, W.D.: Solar wind-magnetosphere energy coupling efficiency and partitioning: Hildcaas and preceding cir storms

during solar cycle 23. Journal of Geophysical Research: Space Physics **119**(4), 2675–2690 (2014)

[6] Siscoe, G., Crooker, N., Clauer, C.: Dst of the carrington storm of 1859. Advances in Space Research **38**(2), 173–179 (2006)

[7] Lyon, J.G.: The solar wind-magnetosphere-ionosphere system. Science **288**(5473), 1987–1991 (2000)

[8] Biktash, L.: Statistical study of solar wind parameters and evolution of dst variations during 19-23 solar cycles in relation with cosmic ray variations. Sun and Geosphere **7**(1), 41–44 (2012)

[9] Tsurutani, B.T., Gonzalez, W.D., Guarnieri, F., Kamide, Y., Zhou, X., Arballo, J.K.: Are high-intensity long-duration continuous ae activity (hildcaa) events substorm expansion events? Journal of Atmospheric and Solar-Terrestrial Physics **66**(2), 167–176 (2004)

[10] Troshichev, O., Dolgacheva, S., Stepanov, N., Sormakov, D.: The pc index variations during 23/24 solar cycles: Relation to solar wind parameters and magnetospheric disturbances. Journal of Geophysical Research: Space Physics **126**(1), 2020–028491 (2021)

[11] Huang, C.-S., Andre, D.A., Sofko, G.J.: Observations of solar wind directly driven auroral electrojets and gravity waves. Journal of Geophysical Research: Space Physics **103**(A10), 23347–23356 (1998)

[12] Torrence, C., Compo, G.P.: A practical guide to wavelet analysis. Bulletin of the American Meteorological society **79**(1), 61–78 (1998)

[13] Grinsted, A., Moore, J.C., Jevrejeva, S.: Application of the cross wavelet transform and wavelet coherence to geophysical time series. Nonlinear processes in geophysics **11**(5/6), 561–566 (2004)

[14] Podladchikova, O., Berghmans, D.: Automated detection of eit waves and dimmings. Solar Physics **228**, 265–284 (2005)

[15] Souza, A.M.d., Echer, E., Bolzan, M., Hajra, R.: A study on the main periodicities in interplanetary magnetic field bz component and geomagnetic ae index during hildcaa events using wavelet analysis. Journal of Atmospheric and Solar-Terrestrial Physics **149**, 81–86 (2016)

[16] Gopinath, S., Prince, P.: Multifractal characteristics of magnetospheric dynamics and their relationship with sunspot cycle. Advances in Space Research **59**(9), 2265–2278 (2017)

[17] Souza, A., Echer, E., Bolzan, M.J.A., Hajra, R.: Cross-correlation and cross-wavelet analyses of the solar wind imf b z and auroral electrojet index ae coupling during hildcaas. In: Annales Geophysicae, vol. 36, pp. 205–211 (2018). Copernicus Publications Göttingen, Germany

[18] Souza Franco, A., Echer, E., José Alves Bolzan, M.: Wavelet analysis of the magnetotail response to solar wind fluctuations during hildcaa events. In: Annales Geophysicae, vol. 37, pp. 919–929 (2019). Copernicus GmbH

[19] Falayi, E., Adewole, A., Adelaja, A., Ogundile, O., Roy-Layinde, T.: Study of non-linear time series and wavelet power spectrum analysis using solar wind parameters and geomagnetic indices. NRIAG Journal of Astronomy and Geophysics **9**(1), 226–237 (2020)

[20] Gautam, S.P., Silwal, A., Poudel, P., Karki, M., Adhikari, B., Chapagain, N.P.: Study of solar wind and interplanetary magnetic field features associated with geomagnetic storms: The cross wavelet approach. Authorea Preprints (2022)

[21] Burton, R.K., McPherron, R., Russell, C.: An empirical relationship between interplanetary conditions and dst. Journal of geophysical research **80**(31), 4204–4214 (1975)

[22] Caswell, J.M.: A nonlinear autoregressive approach to statistical prediction of disturbance storm time geomagnetic fluctuations using solar data. Journal of Signal and Information Processing **2014** (2014)

[23] Revallo, M., Valach, F., Hejda, P., Bochníček, J.: A neural network dst index model driven by input time histories of the solar wind–magnetosphere interaction. Journal of Atmospheric and Solar-Terrestrial Physics **110**, 9–14 (2014)

[24] Lazzús, J., Vega, P., Rojas, P., Salfate, I.: Forecasting the dst index using a swarm-optimized neural network. Space Weather **15**(8), 1068–1089 (2017)

[25] Lethy, A., El-Eraki, M.A., Samy, A., Deebes, H.A.: Prediction of the dst index and analysis of its dependence on solar wind parameters using neural network. Space Weather **16**(9), 1277–1290 (2018)

[26] Davis, J.C.: Statistics and data analysis in geology john wiley and sons. New York, 289–291 (1986)

[27] Bolzan, M.J.A., Rosa, R.R.: Multifractal analysis of interplanetary magnetic field obtained during cme events. In: Annales Geophysicae, vol. 30, pp. 1107–1112 (2012). Copernicus Publications Göttingen, Germany

[28] McPherron, R.L., O'Brien, P.: Predicting geomagnetic activity: The d st index. Geophysical Monograph Series **125**, 339–345 (2001)

[29] O'Brien, T., McPherron, R.: Seasonal and diurnal variation of dst dynamics. Journal of Geophysical Research: Space Physics **107**(A11), 3 (2002)

[30] Spencer, E., Kasturi, P., Patra, S., Horton, W., Mays, M.: Influence of solar wind–magnetosphere coupling functions on the dst index. Journal of Geophysical Research: Space Physics **116**(A12) (2011)

[31] Maltsev, Y.P., Rezhenov, B.: Relation of the dst index to solar wind parameters. Int. J. Geomagn. Aeron **4**(1), 1–9 (2003)

[32] Boaghe, O., Balikhin, M., Billings, S., Alleyne, H.: Identification of nonlinear processes in the magnetospheric dynamics and forecasting of dst index. Journal of Geophysical Research: Space Physics **106**(A12), 30047–30066 (2001)

[33] Akasofu, S.-I.: Relationships between the ae and dst indices during geomagnetic storms. Journal of Geophysical Research: Space Physics **86**(A6), 4820–4822 (1981)